Shallow-Depth Insertion: Peg in Shallow Hole Through Robotic In-Hand Manipulation

Chung Hee Kim and Jungwon Seo

***Abstract*—This letter presents a novel robotic manipulation technique suitable for *shallow-depth insertion*, which refers to the assembly of a relatively thin peg-like object into a hole with a shallow depth, as can be seen in a cell phone battery insertion for example. Our technique features dexterous manipulation actions that combine into a complete insertion operation, as also commonly demonstrated by humans performing the battery insertion task. The quasistatic stability of the presented insertion process is shown by constructing the space of force-closure grasps and manipulation primitives to navigate the space by changing the grasps. Our technique is directly applicable to a simple hardware setting with the conventional parallel-jaw gripper installed on an industrial robot arm. A set of experiments performed with our software demonstrates the effectiveness of our technique with a high success rate.**

***Index Terms*—Dexterous Manipulation, Grasping, Assembly, Grippers and Other End-Effectors.**

I. Introduction

THIS letter investigates a robotic assembly scenario that we call *shallow-depth insertion*. It refers to inserting relatively thin, peg-like parts into relatively shallow holes. This scenario is quite different from the seemingly related, well-studied problem of *peg-in-hole* assembly [1] in terms of the necessity of dexterity, along with the way of grabbing the part. In traditional peg insertion, the peg is grabbed on the sides that will make contact with the wall of the relatively deep hole. This way of holding can be unstable for thin objects, and even impossible to obtain in case the gripper's workspace is too small. In shallow-depth insertion, unless holding the part by applying forces only on its top face is possible (using the suction gripper for example), changing grasps between the possibly multi-fingered gripper and the object will be necessary to eventually detach the fingers from the non-top faces that will be in contact with the faces of the hole. This necessity of dexterity can be a great challenge, unlike the traditional peg insertion in which it is not necessary to change grasps. In general, advanced robotic dexterity is one of the grand challenges in robotics.

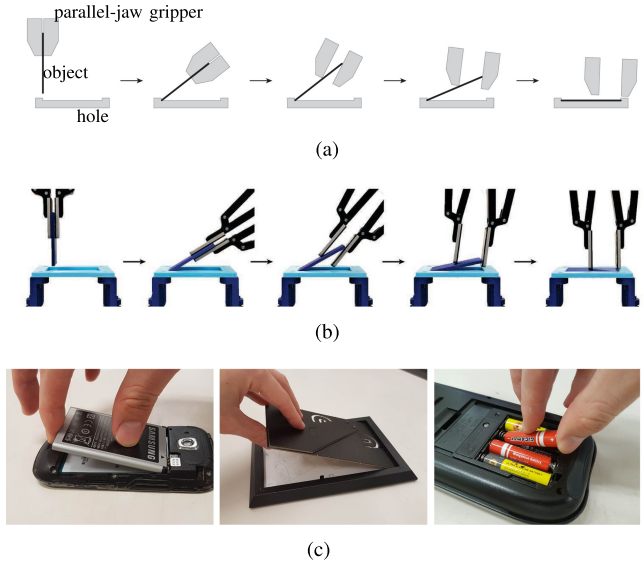

Fig. 1. Our robotic shallow-depth insertion (left to right): (a) schematic and (b) real implementation. (c) Human shallow-depth insertion demonstrated with the cell phone battery, the picture frame, and the dry cell battery.

Our robotic shallow-depth insertion technique to be presented in the paper is schematically shown in Figs. 1(a) and (b). The part is inserted in an asymmetric manner such that one of the tips is first matched with the corner of the hole, and then the other tip is tucked in through dexterous, in-hand manipulation in which the relative configuration of the part and the parallel-jaw gripper keeps changing. The robotic operation can be quite similar to human shallow-depth insertion described in Fig. 1(c). The soundness of our approach will be discussed using a quasistatic mechanics model. While quasistatic approaches including ours may suffer from possibly long cycle times, the non-dynamic nature has the advantage of being safer to operate (minimizing possible damage to the part/robot) and simpler to analyze (correctness and completeness guaranteed through a simple static analysis). Indeed, dynamic and impact loads are often supposed to be suppressed in many assembly tasks.

As will be demonstrated by our experiments, the technique enables the robot equipped with minimalist hardware (the two-fingered parallel-jaw gripper with no tactile sensors) to dexterously fulfill shallow-depth insertion, ranging from household activities such as assembling a picture frame or changing dry

Manuscript received September 9, 2018; accepted December 17, 2018. Date of publication January 1, 2019; date of current version January 11, 2019. This letter was recommended for publication by Associate Editor Y. Zheng and Editor H. Ding upon evaluation of the reviewers' comments. This work was supported in part by Hong Kong Innovation and Technology Fund ITS/018/17FP. *(Corresponding author: Chung Hee Kim.)*

C. Hee Kim is with the Department of Electronic and Computer Engineering, The Hong Kong University of Science and Technology, Clear Water Bay, Hong Kong (e-mail: chkimaa@connect.ust.hk).

J. Seo is with the Departments of Mechanical and Aerospace/Electronic and Computer Engineering, The Hong Kong University of Science and Technology, Clear Water Bay, Hong Kong (e-mail: junseo@ust.hk).

This letter has supplemental downloadable multimedia material available at http://ieeexplore.ieee.org, provided by the authors. This includes one multimedia MP4 format movie clip, showing detailed shallow-depth insertion operations on a variety of scenarios. This material is 15 MB in size. References to video are noted within the paper as "see also the video attachment."

Digital Object Identifier 10.1109/LRA.2018.2890449

cell batteries (Fig. 1(c)) to industrial tasks such as assembling small electronics. Overall, our technique can contribute to enhancing the dexterity and versatility of existing robot platforms including the parallel-jaw gripper, which is rarely used beyond traditional grasp-lift-carry tasks.

We begin by outlining relevant literature (Section II) and present our problem statement (Section III). Section IV presents our shallow-depth insertion technique through dexterous manipulation. Section V demonstrates our technique implemented on a real robot system with a set of experiments.

II. Related Work

The work presented in the paper is concerned with robotic insertion. There is extensive literature on robotic insertion due to its practical importance on a range of applications such as manufacturing/assembly automation. In particular, the conventional peg-in-hole problem has received much attention (see [1] and references therein). The problem is concerned with how peg-like parts can be inserted into relatively deep holes. Here the object of interest is usually completely prehended by a robotic gripper throughout the insertion process with no relative reconfiguration. Critical to the process is to devise control strategies to avoid *wedging* or *jamming* [2]. The *remote center compliance* [3] is a passive mechanical device that can prevent wedging or jamming.

Our insertion scenario features shallow insertion depth, which can commonly be seen in, for example, the task of dry cell battery insertion. This scenario is quite different from the seemingly related, conventional peg-in-hole assembly. In [4], the assembly skills for dry cell battery insertion are modeled and analyzed using a hidden Markov model. With shallow insertion depth, the ability to coordinate the interaction between the object and its environment can be of importance, as can be imagined in the battery insertion task again. Our technique realizes the ability by taking advantage of robotic *in-hand manipulation*, which refers to reconfiguring an object within a robotic hand. Robotic in-hand manipulation is an ongoing challenge, and directly connected with the important issue of robotic dexterity. It has been realized in the forms of robotic regrasping, dexterous manipulation, and finger gaiting [5]–[9]. Our work is particularly relevant to the body of work concerning in-hand manipulation with low degree-of-freedom (DOF) grippers: [10]–[14].

The presented insertion technique is formulated as quasistatic manipulation in which inertial forces are negligible. Robotic grasping/fixturing (see [15] and references therein) and related tasks such as whole-arm grasping (see [16] for example) are fundamental quasistatic manipulation problems. Robotic grasps are characterized by their closure properties such as *force-closure* or *form-closure* [17]. The literature on quasistatic assembly is also relevant to our work; one recent example can be seen in [18]. Pushing is another important quasistatic technique [19]. Other instances include palmar manipulation [20], toppling manipulation [21], pivoting manipulation [22], and push-grasping [23].

III. Problem Description

This letter studies a robotic solution to shallow-depth insertion (recall Fig. 1), which refers to assembling a relatively thin object into the complementary shallow hole. We will examine how to devise and integrate a range of manipulation actions for the successful completion of the insertion task.

The task of shallow-depth insertion is modeled as a quasistatic process because it is common to suppress inertial forces in assembly processes. The task is also modeled as a two-dimensional manipulation process on the plane in that the motions off the plane are often suppressed physically by, for example, the walls of the hole. An *object* of interest can then be modeled as a rigid line segment moving on the plane, and it is manipulated to be inserted into a ⊔-shaped hole with a shallow depth (wider than deep in terms of its aspect ratio). Object deformation is not factored in our analysis because our manipulation technique preserves rigid body constraints. For those objects with sufficiently large stiffness, the influence of deformation on the outcome of the insertion operation can be considered insignificant. Envisioning practical applications, we are interested in using a simple, common robotic gripper—the two-fingered parallel-jaw gripper with one DOF—simply *gripper* for short from this point on. Again, the setting can be seen in Fig. 1.

We initially assume that an object is held by a gripper in a longitudinal manner: the finger surfaces and the line segment of the object are parallel. Otherwise (holding the object by making contacts at the tips), it can kinematically be impossible to grip the object if the opening range of the gripper is less than the length of the object. In addition, such a way of holding might be unsuitable for object stability: unless the two contact points can "see each other" with the friction cones regarded as their "field of view," no force-closure is guaranteed [17]. The longitudinal way of holding renders in-hand manipulation necessary to transition from the initial to the target configuration in which the object is placed in the hole, as depicted in Fig. 1. However, the lack of mobility in the gripper poses a great challenge in performing any in-hand manipulation, other than traditional grasp-lift-carry operations. Our interest is in devising and executing in-hand manipulation actions that will guarantee quasistatic equilibrium all the way through the insertion operation such that the object can be held stably.

IV. Manipulation for Shallow-Depth Insertion

In this section, we present our manipulation strategy for successful shallow-depth insertion, featuring stable in-hand manipulation techniques.

A. Secure Grasps for Shallow-Depth Insertion

Consider the typical relative configuration of the object, the gripper, and the hole that can be observed throughout the insertion process illustrated in Fig. 1. Fig. 2(a) describes the configuration. It can be represented with the three non-dimensionalized parameters $\gamma = \delta/\ell$, θ, and ψ, where δ is the distance between the two contacts at A (between the object and finger #1 of the gripper) and B (between the object and finger #2), ℓ is the length of the object, θ is the angle between the hole and the object, and ψ is the angle between the object and the surface of finger #1. The physical interaction between the object and the environment (the gripper and the hole) during the insertion operation can be modeled with three point contacts at A, B, and G (between

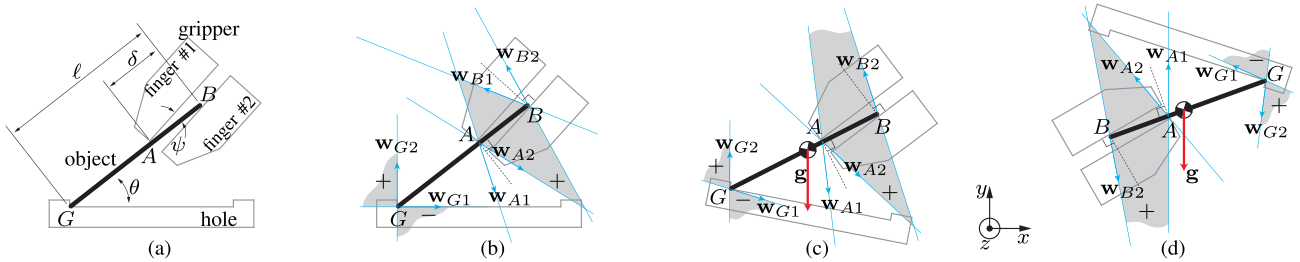

Fig. 2. (a) Configuration of the object, the gripper, and the hole parametrized with ℓ, δ, θ, and ψ. (b) Moment labeling diagram of the configuration featuring the contact wrenches at A, B (frictional contacts) and G (two contact normals). $\mathbf{w}_{(\cdot)}$'s denote unit contact wrenches. (c, d) Moment labeling with (1) friction at G which will make the angle between $\mathbf{w}_{G1}$ and $\mathbf{w}_{G2}$ larger by the friction cone angle, and (2) sliding at B due to **regrasp** which will make only $\mathbf{w}_{B2}$ active. Note that $\mathbf{g}$, the wrench of gravity, is parallel to $\mathbf{w}_{G2}$ and $\mathbf{w}_{A1}$ respectively in (c) and (d).

the tip of the object and the corner of the hole). The contact wrenches at each of the contacts are spanned by multiple unit contact wrenches modeling friction and geometry. In Fig. 2(b), $\mathbf{w}_{A1}$ and $\mathbf{w}_{A2}$ ($\mathbf{w}_{B1}$ and $\mathbf{w}_{B2}$) are the unit contact wrenches that span the friction cone at A (B); G is shown as a frictionless contact with the unit wrenches $\mathbf{w}_{G1}$ and $\mathbf{w}_{G2}$ derived from the two contact normals perpendicular to each other (if frictional, the angle between $\mathbf{w}_{G1}$ and $\mathbf{w}_{G2}$ increases as can be seen in Fig. 2(c) or (d)).

It is possible to hold the object securely in such configurations. This can be seen by considering the force conditions under which force-closure is attainable. Fig. 2(b) visualizes the composite wrench cones of the contact wrenches at A, B, and G, according to the formalism of *moment labeling* [1]. The "+" labeled, shaded quadrilateral between A and B represents the positive linear combinations

$$\mathrm{pos}(\{\mathbf{w}_{A1}, \mathbf{w}_{A2}, \mathbf{w}_{B1}, \mathbf{w}_{B2}\})$$

which is the composite cone of the contact wrenches at A and B. The composite wrench cone at G

$$\mathrm{pos}(\{\mathbf{w}_{G1}, \mathbf{w}_{G2}\})$$

is represented as the "+" and "−" labeled, shaded quadrants at G. The diagram can be read as follows. If the intersection of the shaded regions with the same label is null, the set of all the possible contact wrenches spans the whole three-dimensional wrench space and thus force-closure is obtained [1], [17]. The diagram then suggests that force-closure is attainable if (1) θ is sufficiently small, (2) γ is sufficiently small, (3) ψ is sufficiently large, and (4) friction at contacts A, B, and G is sufficiently large. Otherwise, the two "+" labeled regions can intersect—no force-closure.

The set of all the configurations (γ, θ, ψ) in force-closure, which will be referred to as *grasps* for short, can be visualized in a sampling-based manner. Fig. 3 shows the results. The data points were densely sampled in the $\theta\psi$-space over the entire range of 0° to 90° at a resolution of 1°. γ is varied from 0.1 to 0.9 with steps of 0.1. For each of the $90 \times 90 \times 9$ data points in the $\gamma\theta\psi$-space, force-closure is checked by solving a linear optimization problem as presented in [17]. For each γ, the set of the grasps is represented as the region on the $\theta\psi$-plane under the curve labeled with the value of γ. For example, when $\gamma = 0.8$, the set of the grasps is the union of the area below the $\gamma = 0.9$ curve and the area between the $\gamma = 0.9$ and $\gamma = 0.8$ curves. It can be seen that the set expands as the value of γ decreases.

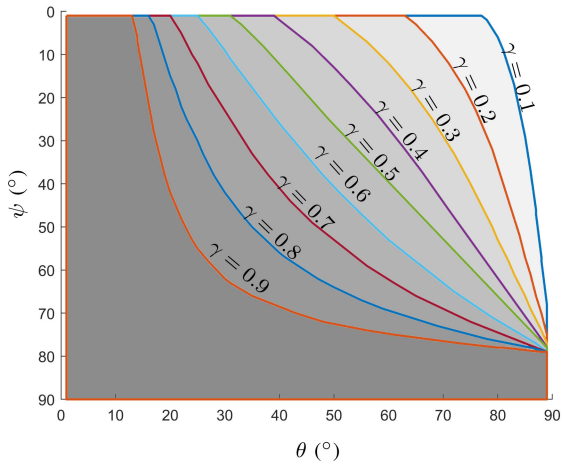

Fig. 3. The collection of secure configurations (γ, θ, ψ), referred to as *grasps*, represented as the areas under the curves, i.e., the ten shades of gray, for increasing values of γ over the $\theta\psi$-plane. Each shaded area includes all the other areas below it. Contacts A and B are assumed to exhibit friction cones with aperture of 0.2rad. Contact G is frictionless.

B. Two Primitive Operations: Tilt and Regrasp

Now we present two types of manipulation primitives, **tilt** and **regrasp**, to navigate the space of the force-closure grasps. These will be useful for executing shallow-depth insertion.

- **tilt** (Fig. 4(a)): Change θ by rotating the gripper-object system about the corner of the hole, G. No change in ψ and the distance between the two fingers.
- **regrasp** (Fig. 4(b)): Change ψ by rotating the gripper about the contact point A (or the tip of finger #1). No change in θ, but the distance between the two fingers has to be coordinated accordingly.

Through the **tilt** (**regrasp**) operation, it is possible to traverse the set of the grasps (shown in Fig. 3) horizontally (vertically) while keeping ψ (θ) constant.

C. Initial Positioning for Shallow-Depth Insertion

Our shallow-depth insertion process begins with initial positioning in which the tip of the object is matched with a corner

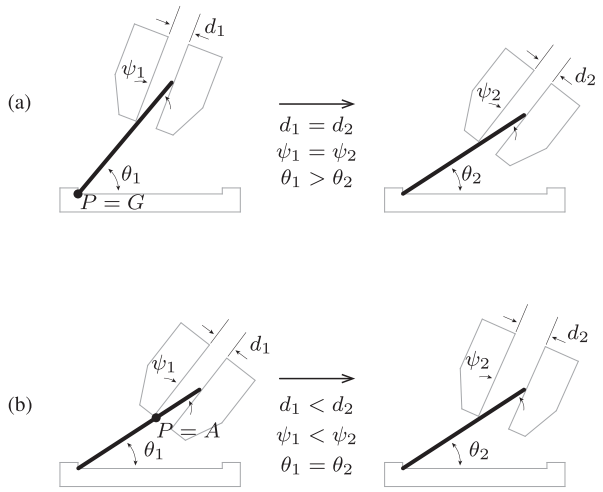

Fig. 4. (a) **tilt** operation. The object-gripper system rotates about the pole $P = G$. (b) **regrasp** operation. The gripper rotates about the pole $P = A$, while opening the fingers accordingly.

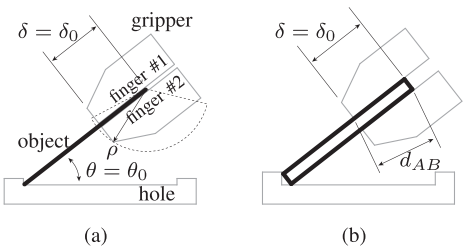

Fig. 5. (a) Initial configuration of the object with (a) negligible and (b) non-negligible thicknesses.

of the hole. In Fig. 5(a), the initial configuration is specified by $\gamma_0 = \delta_0/\ell$ and θ_0. Note, $\psi = 0^\circ$.

First, δ_0 (and thus γ_0) can be chosen to be less than the maximum opening range of the gripper such that **regrasp** can be performed all the way through until $\psi = 90^\circ$. Since it can be hard to change δ once the object is held and squeezed by the gripper, practically δ_0 needs to be fixed before the matching of the corner happens, for example, when the object is picked for the first time. If the thickness of the object is considered non-negligible as illustrated in Fig. 5(b) (relaxed from our assumption in Section III), δ_0 has to be chosen such that the maximum opening range of the gripper is equal to or greater than d_{AB}, the actual distance between the contacts A and B, in order for **regrasp** to be performed completely (here the maximum attainable value of ψ will be less than 90° and can be obtained by simple trigonometry).

Second, given δ_0, θ_0 is then chosen such that $\theta_\ell < \theta_0 < \theta_u$. The lower bound θ_ℓ is determined kinematically such that the area swept by finger #2 during the **regrasp** phase is free from any collision constraints. The area can be approximated by the fan-shaped area (centered at the tip of the object) shown in Fig. 5(a); its radius ρ is determined by the shape of the finger. Note that it is larger than necessary because the distance between the tips of finger #2 and the object keeps decreasing while ψ increases. The upper bound θ_u is determined statically such that force-closure is attained. Recall that in Section IV-A we discussed that θ needs to be sufficiently small for force-closure. Given δ_0 (and thus the corresponding value of γ), Fig. 3 can be applied to find θ_u: θ_u is chosen such that during the **regrasp** operation from $\psi = 0^\circ \rightarrow 90^\circ$, the configuration always remains under the curve, to ensure force-closure. For example, if the friction coefficient at A and B is $\mu = 0.2$, G is frictionless, and γ is set to be 0.4, θ_u is computed to be 39°. The larger the friction at A, B, and G, the larger the upper bound on θ.

If it is impossible to find feasible θ_0 (that is, in case $\theta_u < \theta_\ell$), δ_0 needs to be reduced and θ_0 has to be searched again as explained above. As can be seen in Fig. 3, as γ gets smaller, θ_u can get larger.

D. Towards Complete Shallow-Depth Insertion

We finally address how to complete shallow-depth insertion. Initially, the configuration of the object-gripper-hole system (discussed in Section IV-C) is at the top border of the plot in Fig. 3 because $\psi = 0^\circ$. On successful completion, the gap between the hole and the object vanishes ($\theta \rightarrow 0^\circ$), and the gripper will be separated from the object ($\psi \rightarrow 90^\circ$). The target configuration of the system thus corresponds to the bottom-left corner of the plot. It is possible to take the initial into the target configuration arbitrarily closely by combining the **regrasp** and **tilt** actions: the former (the latter) operation will move the configuration down (left) monotonically in the plot.

The quasistatic stability of the **tilt** phase in which θ decreases monotonically can be confirmed by considering that all the intermediate configurations are in force-closure and there is no change in the contact modes at A, B, and G. During the **regrasp** phase in which ψ increases monotonically, however, the object slips on B and thus only one of the unit contact wrenches at B, $\mathbf{w}_{B2}$, is active. See Figs. 2(c) and (d). If friction at the contacts is sufficiently large, the system can again be in force-closure with the sliding contact at B. If not in force-closure, the two "+" labeled areas necessarily intersect. In this case, we additionally take the wrench of the object weight (the red arrow $\mathbf{g}$ in the negative y-direction) into account to see that the forces can again be in equilibrium. If (1) the line of $\mathbf{g}$ and the intersection of the two "+" labeled areas are disjoint and (2) the line has a negative moment with respect to all the points in the intersection, the wrenches can be in equilibrium, according to the formalism of moment labeling [1], [17]. These are satisfied in a range of hole orientations in which the bottom face of the hole does not have to be level (perpendicular to $\mathbf{g}$): the orientation shown in Fig. 2(c) in which $\mathbf{g}$ is parallel to $\mathbf{w}_{G2}$ (here the intersection must be on the left of $\mathbf{w}_{G2}$) and all the orientations rotated counterclockwise (about the positive z-direction) from Fig. 2(c) to (d) in which $\mathbf{g}$ is parallel to $\mathbf{w}_{A1}$ (here the intersection must be on the left of $\mathbf{w}_{A1}$). Therefore, the system can be in quasistatic equilibrium even when there is relative motion at B. Note that the presented bounds, Figs. 2(c) and (d), estimate the range conservatively.

In practice, it can be necessary to perform a forceful push action to complete the insertion process in case, for example,

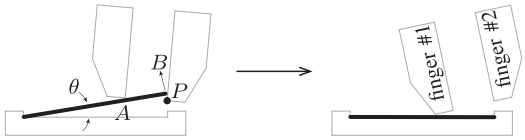

Fig. 6. **tuck** operation. The gripper rotates about the pole P, the tip of finger #2, to bring θ to zero and complete the insertion.

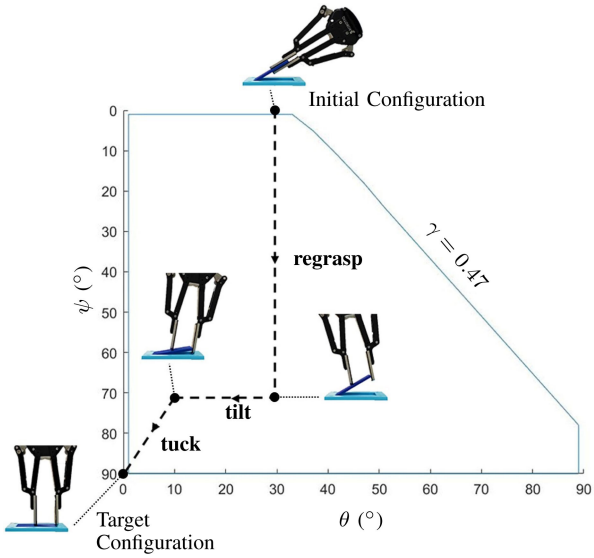

Fig. 7. Object-gripper-hole system navigating through the $\theta\psi$-space via the three primitive operations: **tilt**, **regrasp**, and **tuck**.

the hole is intentionally designed to be smaller than the part. We thus introduce another primitive operation, **tuck**:

- **tuck** (Fig. 6): Change θ and ψ by rotating the gripper about the tip of finger #2.

The **tuck** operation causes finger #1 to push the object downwards at contact A, taking $\theta \to 0°$, and contact B to slide towards the tip of finger #2, taking $\psi \to 90°$.

Fig. 7 shows a final course of manipulation incorporating **tilt**, **regrasp**, and **tuck**. First, the system is manipulated from the initial configuration to a configuration nearby the target configuration through **regrasp** followed by **tilt**. Of course, the **regrasp**-**tilt** motion can either be decomposed further into finer levels of granularity (for example, **regrasp**-**tilt**-**regrasp**-**tilt**-$\cdots$-**regrasp**-**tilt**), or superimposed into one smooth motion if needed. Second, **tuck** is performed to complete the insertion process. One important question is when to transition to **tuck**. It can be addressed in an empirical manner, considering the difficulty in modeling the physical interaction between the object and the hole generally. In the following section, we will present our setting that resulted in successful experiments.

Remark: The robustness of our insertion technique can be established by considering that the quasistatic stability discussed in this section is geometrically guaranteed by separating convex areas. For example, consider uncertainty in modeling friction. Suppose that lower bounds for the uncertain coefficients of friction can be estimated reliably. Our insertion technique can be parametrized using the lower bounds, which will result in the largest possible "+" labeled, convex areas. The resulting operation will then be performed robustly without losing stability because the actual "+" labeled areas will shrink. Methods for increasing robustness—tolerance to such uncertainty—include (1) minimizing δ_0 subjected to $\delta_0 > 0$, which will enlarge the set of force-closure grasps, and (2) minimizing θ_0 subjected to $\theta_0 > \theta_\ell$, which can ensure that manipulation happens in the interior of the set.

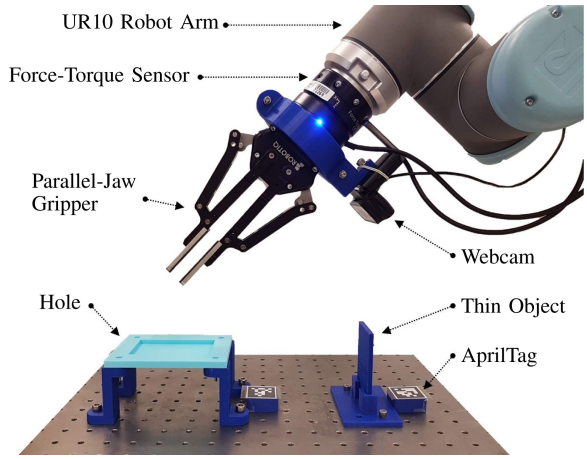

Fig. 8. Our experiment setup featuring the force-torque sensor and webcam attached to the wrist of the robot arm, parallel-jaw gripper, 3D-printed thin object and hole.

V. Implementing Shallow-Depth Insertion

Our shallow-depth insertion technique has been implemented on a real robotic system. A set of experiments were performed to validate the technique.

A. Hardware Setting

Fig. 8 shows our hardware setting with the Robotiq 2-Finger Adaptive parallel-jaw gripper attached to the Universal Robots UR10 six-DOF arm. The sensing modalities of the platform include wrist force-torque sensing using the FT 300 Force Torque Sensor and visual perception using a 1080p webcam.

B. Our Software

Our software[1] implementing shallow-depth insertion with the hardware platform is organized as ROS[2] packages written in Python. The software features three methods, `tilt()`, `regrasp()`, and `tuck()`, corresponding to the three primitives—**tilt**, **regrasp**, and **tuck**—discussed in the previous section. These methods are realized by appropriately coordinating the drivers of the arm and the gripper, Moveit! and robotiq respectively, also available in ROS.

`tilt()`: This method implements the **tilt** operation. It takes as input the position of G (that is, the center of rotation) and the amount of tilting. The gripper is then controlled to perform rigid body rotation with the information. Constructively,

[1]https://github.com/chjohnkim
[2]https://www.ros.org

the method is implemented through the ROS service named `GetCartesianPath`, which is useful for generating and executing parametrized trajectories (in this case, a circular arc parametrized by the center angle).

`regrasp()`: This method implements the **regrasp** operation. It takes as input the position of A (that is, the center of rotation), the desired displacement of ψ, the dimensions of the object and the gripper, and the relative configuration of the object and the gripper. The arm and the gripper are then controlled to increase ψ while θ and the position of A are kept constant. Note that the motions of the arm and the gripper, governed by separate drivers, have to be coordinated because the variables ψ and d (the distance between the fingers) are coupled. It is possible to express the relationship between the variables in closed form, and these equations were incorporated in our software code.

`tuck()`: This method is derived from `tilt()` due to the similarity of the function. The difference is that the gripper is controlled to rotate about the tip of finger #2.

The input arguments of the functions are fed autonomously using the wrist force-torque sensor, the webcam, and the joint encoders of the arm and the gripper, except for the dimension of the task object to be provided by the user and the desired δ_0, θ, ψ values to be provided by our high-level controller (as shown in Fig. 7).

C. Experiments

Our shallow-depth insertion technique was tested on six different objects: 3D-printed card, picture frame, lego block, mobile phone battery, plastic container lid, and a dry cell battery. In addition, vertical insertion (in which the hole is placed on a vertical wall) and expedited insertion (in which the insertion is executed in 7 s in average including 2.5 s for **regrasp**) was performed with the 3D-printed card. For each scenario, 20 trials were conducted totaling to 160 trials. The overall success rate was $154/160 = 96\%$. Table I summarizes the experiment results with our choices for δ_0 and θ_0 determined by considering friction between the materials in contact[3]. Fig. 9 shows the progress of the experiments.

The experiments were performed autonomously as follows; see also the video attachment.

1) Locate Task Object: Initially the task object is standing vertically fixed by an object holder. The configuration of the object is obtained through camera vision via the visual fiducial system AprilTag [24].

2) Grasp Task Object: The gripper moves to a position directly above and pointing down at the task object. It then searches for the task object using the wrist force-torque sensor by moving down until a predefined threshold resistance is reported. The top edge of the task object can then be detected with high accuracy. Once the searching is done, the gripper grasps the object with the desired δ_0 value.

3) Locate Hole: After firmly grasping the task object, the camera searches for the pose of the hole using AprilTag.

[3]The coefficients of friction are from sources on engineering practice so the values are approximate.

4) Approach Hole: The gripper proceeds to move to a position directly above and in between the two corners of the hole. Note that the task object is not making any contact at this point, and is oriented perpendicular to the hole.

5) Make Contact G: The gripper moves down until a vertical threshold resistance is reported by the force-torque sensor. Subsequently, the gripper moves parallel along the surface of the hole until a horizontal threshold resistance is reported by the sensor. Contact G is now established with $\theta = 90^\circ$ and $\psi = 0^\circ$.

6) Tilting to the Initial Configuration: The robot performs the **tilt** operation such that $\theta \rightarrow \theta_0$.

7) Insertion: Shallow-depth insertion is executed by sequentially performing **regrasp** $\rightarrow$ **tilt** $\rightarrow$ **tuck**, as discussed in Fig. 7 and depicted in Fig. 9. The **regrasp** phase terminates at $\psi = 90^\circ - \epsilon_1$, and the **tilt** phase at $\theta = 0^\circ + \epsilon_2$ (see Table I for the values of $\epsilon_{1,2}$).

The insertion scenarios with the lego block, the container lid, and the dry cell battery pose additional difficulty in terms of a series of the male/female components (the lego block), the absence of a well-defined corner for G (the container lid), and the presence of compliance (the spring-loaded battery receptacle). The complications were resolved by generalizing our nominal technique as follows:

Lego Block: To match the male/female components of the lego blocks, a push-slide motion was executed at the end of the process, during the time frame between the last two panels showing the lego experiment in Fig. 9. Note that there are no barriers to keep the lego block from moving sideways, which was the main cause of the three failures reported in Table I.

Plastic Container: The container does not have a concave corner at G, but rather an extrusion to be matched with the lid edge. Before the lid makes contact with the container, **tilt** was executed to facilitate the matching. This happens during the time frame between the first two panels showing the plastic container experiment in Fig. 9.

Dry Cell Battery: Similarly to the plastic container case, the robot performs **tilt** before the battery and the hole make contact. This can be preferable when the thickness becomes significant, which can render the center of rotation for **tilt** ill-defined. Before the final **tuck** action, the spring is compressed by pushing the battery horizontally to fully insert the battery, during the time frame between the fourth and the fifth panels showing the battery experiment in Fig. 9.

D. Discussion

To attain high success rates as reported in Table I, the motions off the plane (along the z-axis in Fig. 2) need to be suppressed well. In all the scenarios in Fig. 9, the parts are essentially confined to moving on the plane due to the walls on the sides of the holes, except for the lego block scenario in which we witnessed three failures. The positioning accuracy of the manipulator and the gripper can also be critical to successful insertion. For example, if δ_0 is not realized with high accuracy initially, the rest of the procedure may not be performed successfully, which can result in losing or damaging the object or the hole. The positioning accuracy of our platform is known to be ± 0.1 mm (according to

TABLE I
EXPERIMENT RESULTS. THE REGRASP TIME IS THE AVERAGE TIME TAKEN FROM $\psi = 0^\circ$ TO $\psi = 90^\circ - \epsilon_1$ (ALONG THE VERTICAL PATH IN FIG. 7)

Task	Object Dimension (mm)	Initial Configuration		Configuration Before Tuck		Regrasp	Success
Scenario	($\ell \times$ thickness)	δ_0 (mm)	θ_0 ($^\circ$)	ϵ_1 ($^\circ$)	ϵ_2 ($^\circ$)	Time (s)	Rate
3D-Printed Card	85×5	40	30	20	10	24	19/20
Picture Frame	177×3	55	30	15	7	26	20/20
Mobile Phone Battery	65×5	21	40	23	10	22	20/20
Lego Block	48×3	15	45	52	20	13	17/20
Container Lid	385×12	36	15	30	3	28	20/20
Dry Cell Battery	49×14	20	45	50	30	14	18/20
Vertical Insertion (3D-Printed Card)	85×5	10	45	45	11	19	20/20
Expedited Insertion (3D-Printed Card)	85×5	20	30	20	5	2.5	20/20

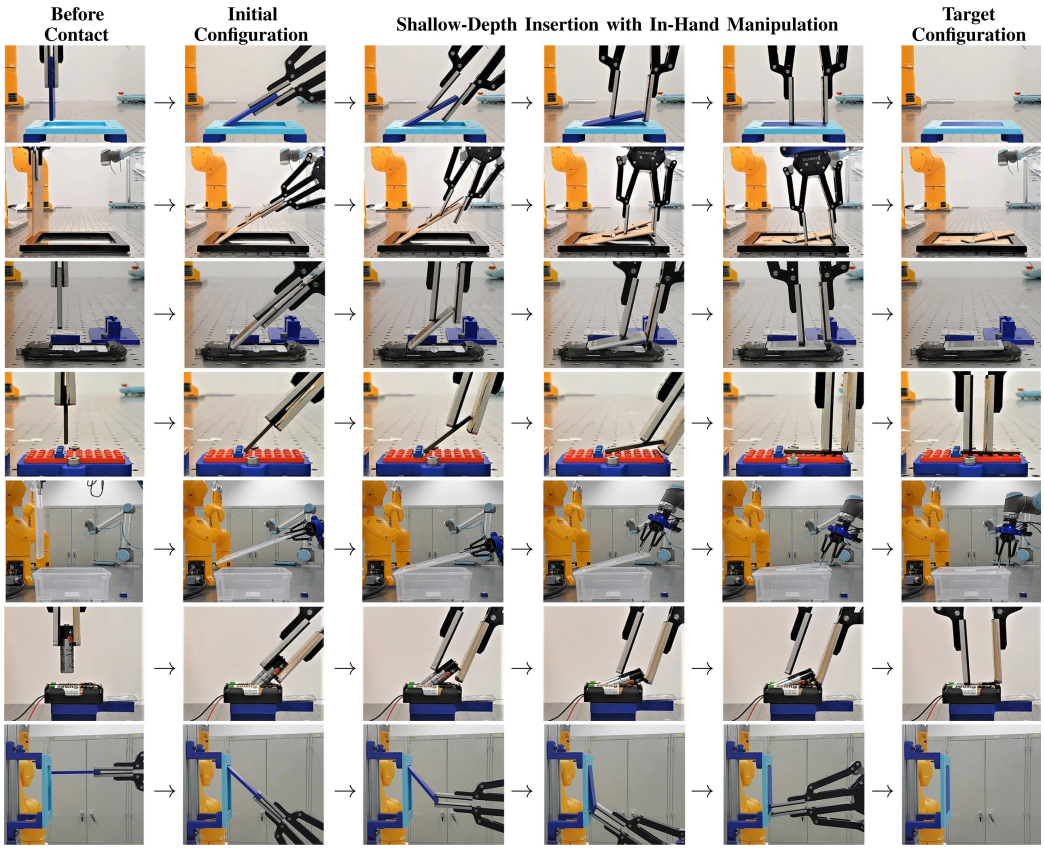

Fig. 9. Each row (from the top) shows the shallow-depth insertion process realized with the 3D-printed card, picture frame, phone battery, lego block, plastic container, and dry cell battery. The bottom row shows vertical insertion in which the hole is on the vertical wall.

the manufacturers), which we believe was sufficient to attain the reported high success rates. Figs. 2(c) and (d) suggest that friction at contact B can be considered insignificant for the stability during **regrasp** because the direction of the contact wrenches at B has no influence on the possibility of force equilibrium in the system orientations between Figs. 2(c) and (d). Based on this consideration, **regrasp** can be expedited and facilitated by having low friction at contact B, with no loss in stability. In our experiments, a smooth tape was applied on the contact surface of finger #2 in order to reduce friction at B (the contact surface of finger #1 is rubber).

One advantage of our insertion technique is repeatable high success rates across a range of scenarios despite the use of noisy sensing, AprilTag, which is known to be sensitive to external factors such as illumination and camera resolution. As can be seen in the experiment procedure, we also adopted force-torque sensing during the course of manipulation actions to reduce uncertainty in positioning. Another advantage is the conservativeness of the analysis. Force-closure is a strong condition for grasp stability. In addition, compliance in the robotic system, which was not modeled in this work, can help enhance stability. As shown in the experiments, our technique also works with holes on a vertical wall. Our analysis in Section IV is not expressive enough to explain this success, which can be attributed to the compliance on the finger contact surface.

The quasistatic nature of our approach may be unsuitable for high-speed execution. It would be hard to attain operation speeds dramatically higher than the "expedited insertion" demonstrated in the experiments, without sacrificing stability. To expedite the process, θ_0 (ϵ_1 and ϵ_2) can be chosen as small (large) as possible to minimize time for **tilt** and **regrasp**. For example, Table I generally shows that the larger the value of ϵ_1 the less the regrasp time. However, doing so can lead into less successful results because the outcome of **tuck** can become more uncertain. In practice, these parameters should be customized to each specific application. At operation speeds higher than the "expedited insertion," a common failure mode is sliding or breaking contact at G. It can be seen that this situation can be ameliorated by decreasing δ_0.

VI. Conclusion

This letter presents a stable, robust robotic manipulation technique for shallow-depth insertion. The usefulness and practicality of our technique was demonstrated through (1) the use of a low-DOF, conventional end-effector, (2) the use of conventional position control scheme, (3) conservative analysis through the adoption of strong conditions such as force-closure, and (4) high success rates with noisy sensing (AprilTag) across a range of insertion scenarios.

Possible directions for future work include adding more sensing modalities and manipulation primitives to address possible failure modes. In practice, the unmodeled positioning uncertainty in the direction perpendicular to the page can result in unsuccessful initial corner matching. Appropriate sensing modalities (vision, for example) may be necessary to enable the robot to perceive the event and abort/retry the process. If the fitting is highly tight, the part can easily get wedged or jammed on the way to the desired initial configuration. Particularly in the direction parallel to the bottom face of the hole, the part may need to be moved a distance as long as its length. This situation, the act of pushing a constrained object using a robot arm, can be considered dual to *prehensile pushing* [25], the act of pushing a grasped object using the environment. Such a manipulation primitive can be combined with our technique to advance robotic shallow-depth insertion.

References

[1] M. T. Mason, *Mechanics of Robotic Manipulation*. Cambridge, MA, USA: MIT Press, Aug. 2001.

[2] S. Simunovic, "Force information in assembly processes," in *Proc. 5th Int. Symp. Ind. Robots*, 1975, pp. 415–431.

[3] P. C. Watson, "Remote center compliance system," US Patent 4098001, Oct. 1976.

[4] N. Yamanobe, H. Fujii, and T. Arai, "Analysis of assembly skills for dry battery insertion based on force control parameters," in *Proc. IEEE Int. Conf. Robot. Biomimetics*, 2009, pp. 191–197.

[5] P. Tournassoud, T. Lozano-Perez, and E. Mazer, "Regrasping," in *Proc. IEEE Int. Conf. Robot. Autom.*, Mar. 1987, vol. 4, pp. 1924–1928.

[6] J. K. Salisbury and J. J. Craig, "Articulated hands: Force control and kinematic issues," *Int. J. Robot. Res.*, vol. 1, no. 1, pp. 4–17, 1982.

[7] L. Han and J. C. Trinkle, "Dextrous manipulation by rolling and finger gaiting," in *Proc. IEEE Int. Conf. Robot. Autom.*, May 1998, vol. 1, pp. 730–735.

[8] A. Bicchi and A. Marigo, "Dexterous grippers: Putting nonholonomy to work for fine manipulation," *Int. J. Robot. Res.*, vol. 21, nos. 5/6, pp. 427–442, 2002.

[9] N. C. Dafle *et al.*, "Extrinsic dexterity: In-hand manipulation with external forces," in *Proc. IEEE Int. Conf. Robot. Autom.*, 2014, pp. 1578–1585.

[10] J. C. Trinkle and R. P. Paul, "Planning for dexterous manipulation with sliding contacts," *Int. J. Robot. Res.*, vol. 9, no. 3, pp. 24–48, 1990.

[11] L. U. Odhner, R. R. Ma, and A. M. Dollar, "Open-loop precision grasping with underactuated hands inspired by a human manipulation strategy," *IEEE Trans. Autom. Sci. Eng.*, vol. 10, no. 3, pp. 625–633, Jul. 2013.

[12] F. Lévesque, B. Sauvet, P. Cardou, and C. Gosselin, "A model-based scooping grasp for the autonomous picking of unknown objects with a two-fingered gripper," *Robot. Auton. Syst.*, vol. 106, pp. 14–25, 2018.

[13] C. Mucchiani, M. Kennedy, M. Yim, and J. Seo, "Object picking through in-hand manipulation using passive end-effectors with zero mobility," *IEEE Robot. Autom. Lett.*, vol. 3, no. 2, pp. 1096–1103, Apr. 2018.

[14] A. Specian, C. Mucchiani, M. Yim, and J. Seo, "Robotic edge-rolling manipulation: A grasp planning approach," *IEEE Robot. Autom. Lett.*, vol. 3, no. 4, pp. 3137–3144, Oct. 2018.

[15] B. Siciliano and O. Khatib, *Springer Handbook of Robotics*. New York, NY, USA: Springer, 2016.

[16] J. Seo, M. Yim, and V. Kumar, "A theory on grasping objects using effectors with curved contact surfaces and its application to whole-arm grasping," *Int. J. Robot. Res.*, vol. 35, no. 9, pp. 1080–1102, 2016.

[17] K. M. Lynch and F. C. Park, *Modern Robotics*. Cambridge, U.K.: Cambridge Univ. Press, 2017.

[18] D. Almeida and Y. Karayiannidis, "Folding assembly by means of dual-arm robotic manipulation," in *Proc. IEEE Int. Conf. Robot. Autom.*, 2016, pp. 3987–3993.

[19] K. M. Lynch and M. T. Mason, "Stable pushing: Mechanics, controllability, and planning," *Int. J. Robot. Res.*, vol. 15, no. 6, pp. 533–556, 1996.

[20] W. H. Huang and G. F. Holden, "Nonprehensile palmar manipulation with a mobile robot," in *Proc. IEEE/RSJ Int. Conf. Intell. Robots Syst. Expanding Societal Role Robotics Next Millennium*, Oct. 2001, vol. 1, pp. 114–119

[21] K. M. Lynch, "Toppling manipulation," in *Proc. IEEE Int. Conf. Robot. Autom.*, May 1999, vol. 4, pp. 2551–2557.

[22] Y. Aiyama, M. Inaba, and H. Inoue, "Pivoting: A new method of graspless manipulation of object by robot fingers," in *Proc. IEEE/RSJ Int. Conf. Intell. Robots Syst.*, Jul. 1993, vol. 1, pp. 136–143.

[23] M. Dogar and S. Srinivasa, "A framework for push-grasping in clutter," in *Proc. Robotics: Sci. Syst. VII*, 2011, vol. 1, pp. 65–72.

[24] E. Olson, "AprilTag: A robust and flexible visual fiducial system," in *Proc. IEEE Int. Conf. Robot. Automat.*, May 2011, pp. 3400–3407.

[25] N. Chavan-Dafle and A. Rodriguez, "Prehensile pushing: In-hand manipulation with push-primitives," in *Proc. IEEE/RSJ Int. Conf. Intell. Robots Syst.*, Sep. 2015, pp. 6215–6222.